New Journal of Physics
The open-access journal for physics

Long quantum channels for high-quality entanglement transfer

L Banchi[1,2], T J G Apollaro[1], A Cuccoli[1,2,3], R Vaia[4,5] and P Verrucchi[1,2,4]

[1] Dipartimento di Fisica, Università di Firenze, Via G Sansone 1, I-50019 Sesto Fiorentino (FI), Italy
[2] INFN, Sezione di Firenze, via G Sansone 1, I-50019 Sesto Fiorentino (FI), Italy
[3] CNISM—Consorzio Nazionale Interuniversitario per le Scienze Fisiche della Materia, Italy
[4] Istituto dei Sistemi Complessi, Consiglio Nazionale delle Ricerche, via Madonna del Piano 10, I-50019 Sesto Fiorentino (FI), Italy
E-mail: ruggero.vaia@isc.cnr.it

New Journal of Physics **13** (2011) 123006 (20pp)
Received 26 May 2011
Published 2 December 2011
Online at http://www.njp.org/
doi:10.1088/1367-2630/13/12/123006

Abstract. High-quality quantum-state and entanglement transfer can be achieved in an unmodulated spin bus operating in the ballistic regime, which occurs when the endpoint qubits A and B are nonperturbatively coupled to the chain by a suitable exchange interaction j_0. Indeed, the transition amplitude characterizing the transfer quality exhibits a maximum for a finite optimal value $j_0^{\rm opt}(N)$, where N is the channel length. We show that $j_0^{\rm opt}(N)$ scales as $N^{-1/6}$ for large N and that it ensures a high-quality entanglement transfer even in the limit of arbitrarily long channels, almost independently of the channel initialization. For instance, for any chain length the average quantum-state transmission fidelity exceeds 90% and decreases very little in a broad neighbourhood of $j_0^{\rm opt}(N)$. We emphasize that, taking the reverse point of view, should j_0 be experimentally constrained, high-quality transfer can still be obtained by adjusting the channel length to its optimal value.

[5] Author to whom any correspondence should be addressed.

Contents

1. Introduction

Quantum state transfer between distant qubits (say, A and B) is a fundamental tool for processing quantum information. The task of covering relatively large distances between the elements of a quantum computer, much larger than the qubit interaction range, can be achieved by means of a suitable communication channel connecting qubits A and B.

Spin chains are among the most studied channel prototypes [1]. In particular, the $S = 1/2$ XY model has been widely employed as a tool for testing and analysing quantum communication protocols. For such a communication channel to be experimentally feasible, one could be led to consider systems with uniform intrachannel interactions [2–9] and whose operation does not require peculiar initialization procedures, although other proposals have recently been put forward [10–13]. On the other hand, the quantum-transfer capabilities of homogeneous spin channels have not yet been fully explored in many respects. For instance, it is a common belief that the longer the chain, the worse the transmission fidelity [1, 2, 14, 15] as an effect of dispersion, and chains up to only a few tenths of spins are often considered. Another class of approaches exploits the possibility of varying the extremal coupling strengths in time [16] and these types of questions have also been studied for networks [17].

This work is devoted to the study of the ballistic regime, where transmission can be depicted [7, 18, 19] in terms of a travelling wavepacket carrying information about the state of the endpoint qubit A, eventually yielding the state reconstruction at the opposite endpoint qubit B thanks to the overall system's mirror symmetry [10–12, 20]. The ballistic regime differs from that arising in the limit of very weak endpoint couplings [3, 5, 6, 21, 22] where (almost) perfect state transfer occurs at very long times as a result of a Rabi-like population transfer involving only two or three single-particle modes. Understanding the basic mechanism

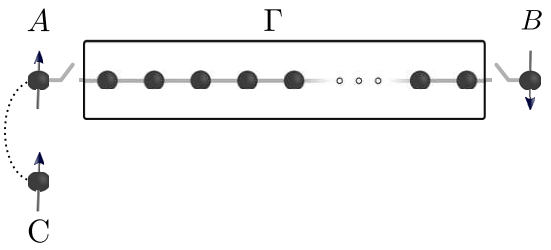

Figure 1. The endpoints of a quantum channel Γ are coupled to the qubits A and B, via the interaction j_0; qubit A can be entangled with an external qubit C.

of ballistic transfer, where the number of involved single-particle modes will be shown to be of the order of $N^{2/3}$, allows us to devise an optimal value of the endpoint interactions for any N, and vice versa. Remarkably, the corresponding transmission quality, as witnessed by the state and the entanglement fidelity, does not decrease to zero when the channel becomes very long, but remains surprisingly high.

We consider the setup illustrated in figure 1: the channel connecting the qubits A and B is a one-dimensional (1D) array of N localized $S = 1/2$ spins with exchange interactions of XX Heisenberg type and a possible external magnetic field applied along the z-direction. This gives the total Hamiltonian the following structure:

$$\mathcal{H} = -\sum_{i=1}^{N-1}(S_i^x S_{i+1}^x + S_i^y S_{i+1}^y) - h\sum_{i=1}^{N} S_i^z - j_0\sum_{i=0,N}(S_i^x S_{i+1}^x + S_i^y S_{i+1}^y) - h_0(S_0^z + S_{N+1}^z), \tag{1}$$

where the qubits A and B sit at the endpoint sites 0 and $N+1$ of a 1D discrete lattice on whose sites $1, 2, \ldots, N$ the spin chain is set. The exchange interaction (chosen as energy unit) and the magnetic field h are homogeneous along the chain, and an overall mirror symmetry is assumed, implying the endpoint coupling j_0 and field h_0 to be the same for both ends. The N spins constituting the XX channel are collectively indicated by Γ. We will focus our attention on how the state of the qubit B evolves under the influence of the chain Γ, and depending on the initial state of the qubit A; the latter is possibly entangled with an ancillary qubit C. The results of the analysis are used to gather insights into quantum-information transmission through the chain so as to characterize the dynamical evolution of the overall system and to maximize the quality of the quantum-state transfer.

Even though the overall scheme could also be used to realize tasks other than quantum information transfer, via the dynamical correlations that the chain induces between A and B [23], our approach is specifically tailored to studying transfer processes along the chain: the qubit B or the qubit pair BC is considered as the target system, depending on whether the quantum state of the qubit A or that of the qubit pair AC is to be transferred, respectively.

In section 2, the formalism used to study the dynamical evolution of the composite system is introduced and we derive the corresponding time-dependent expressions for the quantities used to estimate the quality of the quantum-state and entanglement transfer processes. In section 3, the proposed formalism is applied to the XX model described by (1). In section 4, we put forward an analytical framework in order to improve the understanding of the conditions inducing optimal ballistic dynamics. The resulting high-quality transfer processes along the spin chain are analysed in section 5. The conclusions drawn are presented in section 6, where comments about possible implementations of the procedure are also given. Relevant details of calculations can be found in the appendices.

2. Dynamics and transfer quality

2.1. Dynamics

In this paper, we will essentially focus on the dynamics of the qubit B as described by its time-dependent density operator $\rho^{\mathrm{B}}(t)$. Referring to the specific setup described in figure 1 we prepare the overall system $\mathrm{A} \cup \Gamma \cup \mathrm{B}$ in the initial state $\rho^{\mathrm{tot}} = \rho^{\mathrm{A}} \otimes \rho^{\Gamma} \otimes \rho^{\mathrm{B}}$ and let it evolve into $\mathrm{e}^{-\mathrm{i}\mathcal{H}t}\rho^{\mathrm{tot}}\,\mathrm{e}^{\mathrm{i}\mathcal{H}t}$, where $\mathcal{H}$ is the total Hamiltonian (1), entailing that B evolves according to $\rho^{\mathrm{B}}(t) = \mathrm{Tr}_{\mathrm{A}\cup\Gamma}[\mathrm{e}^{-\mathrm{i}\mathcal{H}t}\rho^{\mathrm{tot}}\,\mathrm{e}^{\mathrm{i}\mathcal{H}t}]$. Since ρ^{tot} has a fully separable structure, $\rho^{\mathrm{B}}(t)$ can be expressed as a linear function of the input density matrix for the qubit A, $\rho^{\mathrm{A}}(0)$:

$$\rho^{\mathrm{B}}(t) = \mathcal{E}_t\ \rho^{\mathrm{A}}(0), \tag{2}$$

where the quantum operation $\mathcal{E}_t$ is a trace-preserving, completely positive, convex-linear map (see, e.g., [24]). Actually, an initial state structure such as $\rho^{\mathrm{A}} \otimes \rho^{\Gamma\mathrm{B}}$ would equally work for the explicit determination of $\mathcal{E}_t$: the separability between ρ^{B} and ρ^{Γ} is adopted just in view of the assumed physical separability of the systems playing the role of sender, medium and receiver. It can be easily shown that the effect of the linear map can be represented in terms of a 4×4 time-dependent matrix

$$T_{\mu\nu}(t) = \mathrm{Tr}[\zeta_\mu^\dagger\ \mathcal{E}_t\ \zeta_\nu], \tag{3}$$

where $\{\zeta_\mu\}$ is an orthonormal basis in the Hilbert space of 2×2 matrices endowed with the Hilbert–Schmidt trace product, $\mathrm{Tr}[\zeta_\mu^\dagger \zeta_\nu] = \delta_{\mu\nu}$. We use indices μ, ν, λ running from 1 to 4, understanding summation over any repeated index, e.g. $\delta_{\mu\mu} = 4$. As the initial state of the qubit A does not enter the expression of $T_{\mu\nu}(t)$, this procedure lies in the framework of general tomographic approaches.

Let us now consider the time evolution of the quantum state describing the qubit pair $\mathrm{C} \cup \mathrm{B}$ when the total system is initially prepared in the state $\rho^{\mathrm{tot}} = \rho^{\mathrm{CA}} \otimes \rho^{\Gamma} \otimes \rho^{\mathrm{B}}$. It can be shown that $T_{\mu\nu}(t)$ is the only ingredient needed for deriving not only the dynamics of the qubit B, but also that of the qubit pair $\mathrm{C} \cup \mathrm{B}$, provided the pair $\mathrm{C} \cup \mathrm{A}$ was prepared separately from the rest of the system, and C is noninteracting [25]. In particular, if C and A are initially prepared in one of the Bell states, say $(|00\rangle + |11\rangle)/\sqrt{2}$, it is

$$\rho^{\mathrm{CA}}_{\mathrm{Bell}} = \tfrac{1}{2}\ \zeta_\mu \otimes \zeta_\mu \tag{4}$$

and hence

$$\rho^{\mathrm{CB}}_{\mathrm{Bell}}(t) = \tfrac{1}{2}\ T_{\nu\mu}(t)\ \zeta_\mu \otimes \zeta_\nu. \tag{5}$$

When both the total Hamiltonian and the initial state $\rho^{\Gamma} \otimes \rho^{\mathrm{B}}$ are symmetric under rotations around the z-axis, it is

$$T_{\mu 2} = T_{2\mu} = T_{22}\ \delta_{\mu 2}, \quad T_{\mu 3} = T_{3\mu} = T_{33}\ \delta_{\mu 3}, \tag{6}$$

and only three matrix elements, say T_{11}, T_{22} and T_{44}, need to be determined.

2.2. Quality of transfer processes

In order to study the quality of the transfer processes mediated by the spin chain, we specifically consider the entanglement transfer from $\mathrm{C} \cup \mathrm{A}$ to $\mathrm{C} \cup \mathrm{B}$ when the former spin pair is initially

prepared in a Bell state (4). The entanglement fidelity

$$\mathcal{F}_{\rm ent}^{\rm Bell}(t) = \tfrac{1}{4}\, T_{\mu\mu}(t) \tag{7}$$

measures the quality of entanglement transmission, i.e. how close the state of C ∪ B at time t is to the initial state of C ∪ A, while the entanglement of the pair C ∪ B is measured by

$$\mathcal{C}_{\rm CB}^{\rm Bell}(t) = \tfrac{1}{2}\, \mathcal{C}[T_{\nu\mu}(t)\, \zeta_\mu \otimes \zeta_\nu], \tag{8}$$

where $\mathcal{C}[\rho]$ is the concurrence [26] between two qubits in the state ρ. Note that (5), (7) and (8) are independent of which Bell state is chosen, since different Bell states are connected to $(|00\rangle + |11\rangle)/\sqrt{2}$ by unitary operations on C, which is isolated.

Another relevant tool for evaluating the quality of the transfer processes is the fidelity of transmission from A to B, which reads $\mathcal{F}_{\rm AB}(t) \equiv {\rm Tr}[\rho^{\rm A\,\dagger} \rho^{\rm B}(t)]$ provided that $\rho^{\rm A}$ is a pure state. If A is initially prepared in the generic state $|\psi_{\theta\varphi}\rangle = \cos\frac{\theta}{2}|0\rangle + {\rm e}^{{\rm i}\varphi} \sin\frac{\theta}{2}|1\rangle$, the fidelity can be averaged over all possible initial pure states by integrating over the Bloch sphere, resulting in the average fidelity

$$\overline{\mathcal{F}}_{\rm AB}(t) = \tfrac{1}{3} + \tfrac{1}{6}\, T_{\mu\mu}(t), \tag{9}$$

which can be compared with (7) to obtain the relation $\overline{\mathcal{F}}_{\rm AB}(t) = \frac{1}{3} + \frac{2}{3}\, \mathcal{F}_{\rm ent}^{\rm Bell}(t)$ [27, 28]. It is worth noting that a high average fidelity could still allow for states that are poorly (or even not at all) transferred, while the ultimate goal is the transmission of *any* state: one can then consider the minimum fidelity $\mathcal{F}_{\rm AB}^{\rm min}(t)$, derived by minimizing with respect to $|\psi_{\theta\varphi}\rangle$, a straightforward task in the presence of z-rotation symmetry (6).

3. The *XX* model

3.1. Dynamical evolution

In this section, we specifically consider the Hamiltonian (1). The system A ∪ Γ ∪ B is prepared in the state $\rho^{\rm tot} = \rho^{\rm A} \otimes \rho^{\Gamma} \otimes \rho^{\rm B}$ where ρ^{Γ} is any state invariant under rotations around the z-axis and $\rho^{\rm B} = b_1\zeta_1 + b_4\zeta_4$: this choice fulfils the requisite of $U(1)$ symmetry of $\rho^{\Gamma} \otimes \rho^{\rm B}$ leading to (6). Referring to the usual Jordan–Wigner transformation, we cast (1) in the fermionic quadratic form

$$\mathcal{H} = \sum_{i,j=0}^{N+1} c_i^\dagger\, \Omega_{ij}\, c_j = \sum_{n=1}^{N+2} \omega_n\, c_n^\dagger c_n, \tag{10}$$

where $\{c_i, c_i^\dagger\}$ are fermionic operators whose nearest-neighbour interaction is described by the $(N+2) \times (N+2)$ tridiagonal mirror-symmetric matrix $\Omega = \{\Omega_{ij}\}$ (see appendix A); an orthogonal transformation $\mathcal{O} = \{O_{ni}\}$ diagonalizes Ω and hence $\mathcal{H}$ [29, 30]. The trivial time evolution of the c_n's entails a time-dependent transformation

$$c_i(t) = \sum_{i=0}^{N+1} U_{ij}(t)\, c_j, \tag{11}$$

where

$$U_{ij}(t) = \sum_n \mathcal{O}_{ni}\mathcal{O}_{nj}{\rm e}^{-{\rm i}\omega_n t}. \tag{12}$$

Provided that (6) hold, we find that

$$\begin{aligned} T_{11}(t) &= |u(t)|^2 + v(t), \\ T_{44}(t) &= 1 - v(t), \\ T_{22}(t) &= -p\langle\sigma^z_{N+1}\rangle\, u(t)\mathrm{e}^{\mathrm{i}\alpha(t)}, \end{aligned} \tag{13}$$

where

$$u(t) = |U_{N+1,0}(t)|, \quad \alpha(t) = \arg[U_{N+1,0}(t)], \tag{14}$$

$$v(t) = |U_{N+1,N+1}(t)|^2 \frac{\langle\sigma^z_{N+1}\rangle + 1}{2} + C_{N+1}(t), \tag{15}$$

$$C_i(t) = \sum_{j,j'=1}^{N} U^*_{ij}(t) U_{ij'}(t)\, \mathrm{Tr}[\rho^\Gamma c^\dagger_j c_{j'}], \tag{16}$$

with $p = \mathrm{Tr}[P\rho^\Gamma]$, and $P = \exp(\mathrm{i}\pi \sum_{i=1}^N c^\dagger_i c_i) \equiv \prod_{i=1}^N (-\sigma^z_i)$ is the chain parity operator, which is a constant of motion. The dynamics of the qubit B and of the qubit pair C ∪ B follow from the above expressions. The time evolution of the magnetization along the chain can also be straightforwardly obtained:

$$\langle\sigma^z_i(t)\rangle = |U_{i0}(t)|^2\langle\sigma^z_0\rangle + |U_{i,N+1}(t)|^2\langle\sigma^z_{N+1}\rangle + G_i(t), \tag{17}$$

where $G_i(t) = 2C_i(t) + |U_{N+1,0}|^2 + |U_{N+1,N+1}|^2 - 1$.

3.2. Fidelities and concurrence

We again consider the system ruled by the Hamiltonian (1) in the setup described above, so that (6) hold. Using (13) we find the entanglement fidelity and the average transmission fidelity of pure states

$$\mathcal{F}^{\mathrm{Bell}}_{\mathrm{ent}}(t) = \tfrac{1}{4} + \tfrac{1}{4}u^2(t) - \tfrac{1}{2}p\cos\alpha\,\langle\sigma^z_{N+1}\rangle\, u(t), \tag{18}$$

$$\overline{\mathcal{F}}^{\mathrm{pure}}_{AB}(t) = \tfrac{1}{2} + \tfrac{1}{6}u^2(t) - \tfrac{1}{3}p\cos\alpha\,\langle\sigma^z_{N+1}\rangle\, u(t), \tag{19}$$

as well as the concurrence

$$\mathcal{C}^{\mathrm{Bell}}_{\mathrm{CB}}(t) = \max\{0, \mathcal{C}_0\}, \tag{20}$$

where

$$\mathcal{C}_0 = |p\langle\sigma^z_{N+1}\rangle|\, u(t) - \sqrt{v(t)[1 - u^2(t) - v(t)]}. \tag{21}$$

From the above formulae it appears that the choice of the initial state $\rho^\Gamma \otimes \rho^\mathrm{B}$ plays an important role [31]: in particular, in order to get the largest concurrence it must be

$$p\langle\sigma^z_{N+1}\rangle = \pm 1, \tag{22}$$

meaning that ρ^Γ is an eigenstate of P and the qubit B is initially in a polarized state, $\rho^\mathrm{B} = \zeta_1$ or $\rho^\mathrm{B} = \zeta_4$; as for the initial state of the channel, the choices range, for example, from its ground state to a fully polarized state. Such a limitation in the choice of the initial state might be overcome by applying a two-qubit encoding and decoding on states ρ^A and ρ^B, respectively [22, 32]. Similarly, for the transmission fidelity to be largest, the condition

$$-p\langle\sigma^z_{N+1}\rangle\cos\alpha = 1 \tag{23}$$

must hold. Note that the lhs of (23) follows from the rotation around the z-axis undergone by the state during the transmission and can be treated by choosing a proper magnetic field [2] or the parity of N, as well as by applying a counter-rotation on the qubit B [31].

The above analysis shows that, once condition (23) is fulfilled, the quality of the state and entanglement transfer mainly depends on $u(t)$ and increases with it.

4. Optimal dynamics

4.1. Transition amplitude

We now have the tools for determining the conditions for a dynamical evolution that corresponds to the best quality of the transmission processes. In appendix A, the algebraic problem of diagonalizing the XX Hamiltonian in the case of nonuniform mirror-symmetric endpoint interactions (A.1) is analytically solved. The eigenvalues of the matrix Ω can be written as

$$\omega_k = -h - \cos k, \tag{24}$$

in terms of the pseudo-wavevector k, which takes $N+2$ discrete values k_n in the interval $(0, \pi)$: from (A.15) and (A.16) it follows that these values obey

$$k_n = \frac{\pi\, n + 2\varphi_{k_n}}{N+3} \quad (n = 1, \ldots, N+2), \tag{25}$$

with

$$\varphi_k = k - \cot^{-1}\left(\frac{\cot k}{\Delta}\right) \quad \in (-\tfrac{\pi}{2}, \tfrac{\pi}{2}), \tag{26}$$

$$\Delta = \frac{j_0^2}{2 - j_0^2}, \tag{27}$$

where we have set $h_0 = h$. From the above equations it follows that the k's correspond to the equispaced values $\pi n/(N+3)$, slightly shifted towards $\pi/2$ of a quantity that is smaller than $\pi/(N+3)$, so that their order is preserved: therefore k can be used as an alternative index for n, understanding that it takes the values k_n, as done in (24). According to the conclusions of the previous section, we focus on the transition amplitude (12) and (14), which explicitly reads

$$U_{N+1,0}(t) \equiv u(t)\, \mathrm{e}^{\mathrm{i}\alpha(t)} = -\sum_n \rho(k_n)\, \mathrm{e}^{\mathrm{i}(\pi n - \omega_{k_n} t)}, \tag{28}$$

where, after (A.21), it is

$$\rho(k) = \frac{1}{N+3-2\varphi_k'}\, \frac{\Delta(1+\Delta)}{\Delta^2 + \cot^2 k}, \tag{29}$$

and mirror symmetry is exploited according to (A.3): the transition amplitude above is a superposition of phase factors with normalized weights, $\sum_n \rho(k_n) = 1$, entailing $u(t) \leqslant 1$, with equality holding when all phases are equal. The distribution $\rho(k)$ is peaked at $k = k_0 = \pi/2$ and its width is characterized by the parameter Δ (27) so that the smaller j_0 the narrower $\rho(k)$.

As $u(t)$ essentially measures the state-transfer quality, the condition for maximizing it at some time t^*, i.e. $u(t^*) \simeq 1$, is that all phases $\pi n - \omega_{k_n} t^*$ are almost equal to each other. Assume

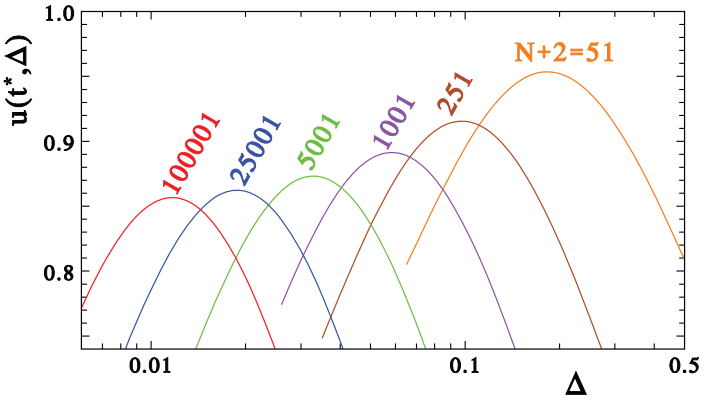

Figure 2. Value of $u(t^*, \Delta)$ as a function of Δ for different wire lengths N. t^* is obtained numerically by maximizing (28) around $t \simeq N+3$. These curves are very well fitted by the function $u(\Delta) = u^{\text{opt}} - c[\ln(\Delta/\Delta^{\text{opt}})]^2$, with c ranging from ~0.17 (low N) to ~0.21 (large N).

for a moment that the k's be equispaced values, as in (A.8), and that the dispersion relation be linear, $\omega_k = vk$; then (28) would read

$$u(t) = \left| \sum_n \rho(k_n)\, \mathrm{e}^{\mathrm{i}\pi n(1-t/t^*)} \right|, \tag{30}$$

with $t^* = (N+3)/v$, so that $u(t^*) = \sum_n \rho(k_n) = 1$, i.e. all modes give a coherent contribution and entail perfect transfer. On the other hand, in our case ω_k is nonlinear in k, and the k_n are not equally spaced due to the phase shifts (26) entering (25), so generally the different modes undergo dispersion and lose coherence.

4.2. Transfer regimes

The dependence of Δ upon j_0 reveals the possibility of identifying different dynamical regimes, characterized by a qualitatively different distribution $\rho(k)$ (29) and hence, as for the transfer processes, different behaviour of the transition amplitude $u(t)$. For extremely small j_0 the distribution $\rho(k)$ can be so thin that (for even N) only two opposite small eigenvalues come into play, say differing by $\delta\omega$, and perfect transmission will be attained at a large time $t = \pi(\delta\omega)^{-1}$ (for odd N there is a third vanishing eigenvalue at $k = \pi/2$ and still two identical spacings $\delta\omega$ do matter). This is the Rabi-like regime also mentioned in the introduction section.

A different regime is observed when j_0 is increased: a few more eigenvalues come into play and it may occur, in a seemingly random way, that their spacings are (almost) commensurate with each other, i.e. they can be approximated as fractions with the same denominator K, yielding phase coherence at $t_K = \pi K$. By recording the maximum of $u(t)$ over a fixed large time interval T, as j_0 is varied (see [3]), a rapid and chaotic variation is observed. This regime is clearly useless for the purpose of quantum communication.

As j_0 further increases, the ballistic regime eventually manifests itself: $\rho(k)$ involves so many modes that commensurability is practically impossible, and more regular behaviour with short transmission time $t^* \sim N$ sets in. The ballistic regime is characterized by relatively large values of $u(t^*, \Delta)$, which is the quantity plotted in figure 2, reporting numerical results for

Table 1. Optimal values $\Delta^{\rm opt}$ and the corresponding $j_0^{\rm opt}$ and $u(t^*, \Delta^{\rm opt})$ (see text for details) for different N.

$N+2$	$\Delta^{\rm opt}$	$j_0^{\rm opt}$	$u(t^*, \Delta^{\rm opt})$
25	0.243	0.625	0.968
51	0.181	0.554	0.949
101	0.138	0.493	0.932
251	0.098	0.422	0.913
501	0.075	0.374	0.900
1 001	0.058	0.332	0.890
2 501	0.042	0.284	0.879
5 001	0.033	0.252	0.873
10 001	0.026	0.224	0.868
25 001	0.0188	0.192	0.862
50 001	0.0148	0.171	0.859
100 001	0.0117	0.152	0.857
250 001	0.0086	0.1303	0.854
500 001	0.0068	0.1160	0.853

increasing chain lengths. It appears that each curve shows a maximum for a particular *optimal* value of $\Delta = \Delta^{\rm opt}(N)$ or, equivalently, of $j_0 = j_0^{\rm opt}(N)$: such maxima are remarkably stable for very high N and yield a very high transmission quality. In table 1, we report some of the optimal values $\Delta^{\rm opt}(N)$ and $j_0^{\rm opt}(N)$ for a wide interval of chain lengths. This last 'ballistic-transfer' regime is the one we are interested in, since it has three strong advantages: firstly, the transmission time $t^* \sim N$ is the shortest attainable; secondly, the maximum value $u(t^*, \Delta^{\rm opt})$ of $u(t^*, \Delta)$ is such that one can achieve very good state transfer, e.g. the corresponding transmission fidelity is far beyond the classical threshold, even for very long chains; thirdly, it is not necessary to fine-tune j_0 to $j_0^{\rm opt}$, since from the data set reported in figure 2 it can be estimated that the relative loss in amplitude is $u^{\rm opt} - u(j_0^{\rm opt} \pm \delta j_0) \simeq 0.8(\delta j_0/j_0^{\rm opt})^2$, e.g. a 15% mismatch in j_0 results in a loss of less than 2% in the transition amplitude.

The above analysis gives a physical interpretation of what is observed in figure 3 of [3], where the Rabi-like, intermediate and ballistic regimes emerge.

A qualitative picture of the ballistic regime can be obtained by viewing the transition amplitude (28) as a wavepacket with $N+2$ components. It can be evaluated by progressively adding the contributions from symmetric eigenvalues, i.e. for odd N summing between $(N+1)/2 \mp \ell$, for $\ell = 0,\ 1, \ldots, (N+1)/2$. This yields the partial sum $u_\ell(t^*)$ shown in figure 3, together with the corresponding frequency and density. One can see that the amplitude increases only over the modes of the linear-frequency zone, i.e. where frequencies are equally spaced, indicating that only those wavepacket components whose frequency lies in such a zone play a role in the transmission process.

4.3. Ballistic regime and optimal values

From the above reasoning, since the modes contributing to the amplitude lie in a range of sizes Δ around k_0, in order to get high-quality transfer processes it is necessary that the corresponding frequencies be almost equally spaced, meaning that ω_{k_n} is approximately linear in n. Actually,

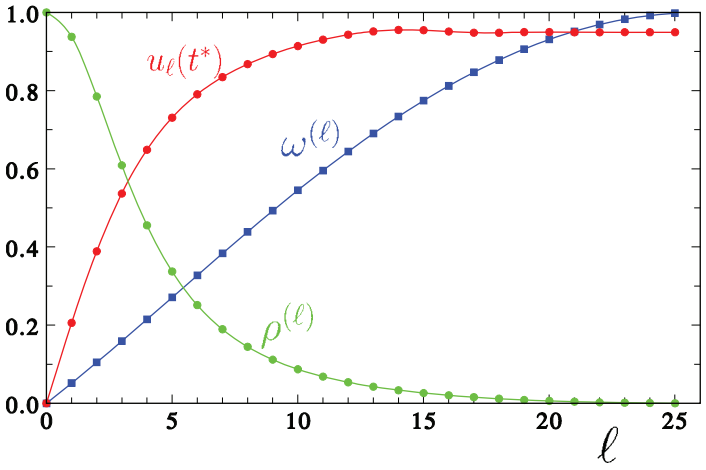

Figure 3. Partial sum of the amplitude $u_\ell(t^*)$ versus ℓ for $N+2=51$ and $j_0=0.58$, together with the corresponding frequency and density.

ω_k has an inflection point in k_0: its nonlinearity is of the third order in $k-k_0$ and the modes close to k_0 satisfy the required condition. However, from the phase shifts (26) a further cubic term arises, which depends on Δ. As Δ varies with j_0, the latter can be chosen so as to eliminate the cubic terms, yielding a wide interval with almost constant frequency spacing. The latter can be expressed just as the derivative of ω_{k_n} with respect to n, $\partial_n\omega_{k_n}=\sin k\,\partial_n k$. The last term is evaluated from (25) and (26),

$$\partial_n k=\frac{\pi+2\varphi_k'\partial_n k}{N+3}=\frac{\pi}{N+3-2\varphi_k'}, \tag{31}$$

$$\varphi_k'=-\frac{1-\Delta}{\Delta}+\frac{(1-\Delta^2)\cos^2 k}{\Delta[\Delta^2+(1-\Delta^2)\cos^2 k]}, \tag{32}$$

so that

$$\begin{aligned}\partial_n\omega_{k_n}&=\frac{\pi\ \sin k}{N+3-2\varphi_k'}\\&=\frac{\pi}{t^*}\left[1+\left(2\,\frac{1-\Delta^2}{t^*\Delta^3}-\frac{1}{2}\right)\cos^2 k+\mathrm{O}(\cos^4 k)\right],\end{aligned} \tag{33}$$

where $t^*=N+3+2\,(1-\Delta)/\Delta$ is the arrival time. It follows that one can minimize the nonlinearity of ω_{k_n} by setting the width to the value Δ_0 satisfying

$$\Delta_0=\left[\frac{4}{t^*}\,(1-\Delta_0^2)\right]^{1/3}\underset{N\gg1}{\longrightarrow}2^{2/3}N^{-1/3}, \tag{34}$$

and $j_0\simeq 2^{5/6}N^{-1/6}$ for large N. Therefore the main mechanism that produces an optimal ballistic transmission is that of varying the endpoint exchange parameter to the value j_0 that 'linearizes' the dispersion relation. Actually, if the corresponding $\Delta_0=\Delta(j_0)$ is such that $\rho(k)$ exceeds the region of linearity, further gain arises by lowering j_0 so as to tighten the relevant modes towards k_0. However, at the same time, ω_{k_n} becomes less linear and the trade-off between these two effects explains why a maximum is observed. This is apparent in figure 4, where for different values of Δ the shapes of $\partial_n\omega_k$ can be compared with the excitation density $\rho(k)$: for

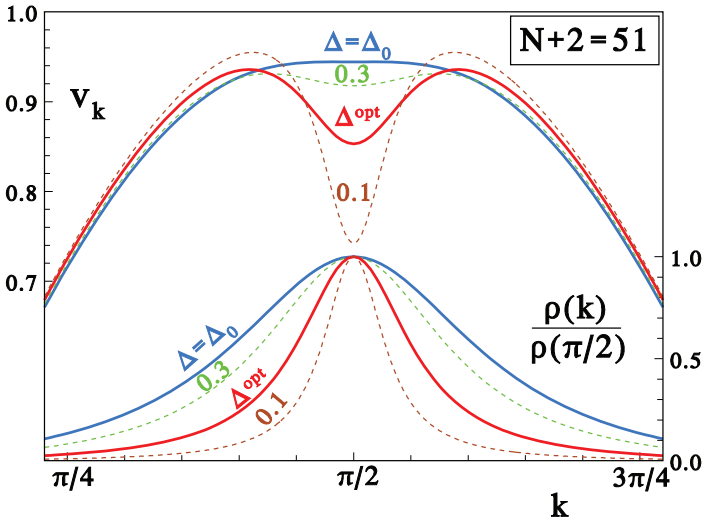

Figure 4. The 'group velocity' $v_k \equiv [(N+3)/\pi]\partial_n \omega_{k_n}$ and $\rho(k)$ versus k for different values of Δ. The thicker curves correspond to $\Delta_0 = 0.3944$ (34) that gives the flat behaviour at k_0 and to $\Delta^{\rm opt} \simeq 0.1825$.

$\Delta = \Delta_0$ the density still has important wings in the nonlinear zone, so the optimal value $\Delta^{\rm opt}$ turns out to be smaller.

The dynamics in the ballistic regime is best illustrated by the time evolution of the magnetization (17) along the chain, plotted in figure 5 when the initial state is $|\uparrow\rangle \otimes |\downarrow\downarrow\cdots\downarrow\rangle \otimes |\uparrow\rangle$. The initial magnetizations at the endpoints generate two travelling wave-packets: for nonoptimal coupling ($j_0 = 1$, upper panel) they change their shape and quickly straggle along the chain; for optimal coupling ($j_0 = j_0^{\rm opt}$, lower panel) they travel with minimal dispersion. This confirms that the coherence is best preserved when the optimal ballistic dynamics is induced: in the next section we show that such dynamics do in fact correspond to high values of the quality estimators for the state and entanglement transfer.

5. Information transmission exploiting optimal dynamics

The requirement (23) means that the state is not rotated by the dynamics when it arrives on site B, although during the evolution it may undergo a rotation around the z-axis. In [23], it has been shown that $\alpha = -\frac{\pi}{2}(N+1)$ at the transmission time t^*. Therefore, also without applying a counter-rotation on qubit B [31], condition (23) can be fulfilled by choosing $N = 4M \pm 1$, where the sign $\pm$ is given by (22) and thus depends on the initial state of the chain. In the following, we assume that conditions (22) and (23) are always satisfied.

Let us consider for the moment that Γ and B are initially in the fully polarized state $|\downarrow\downarrow\cdots\downarrow\rangle \otimes |\downarrow\rangle$. In that case $v(t) \equiv 0$ and the transmission fidelities (18) and (19), as well as the concurrence (20), only depend on, and monotonically increase with, $u(t)$. The best attainable information-transfer quality corresponds therefore to the maximum amplitude $u_{\rm opt} \equiv u(t^*, \Delta^{\rm opt})$. In figure 6 and table 1 we report these values together with the corresponding optimal $\Delta^{\rm opt}$ as a function of the chain length N in a logarithmic scale; the inset shows that $\Delta^{\rm opt}$ obeys the same power-law behaviour predicted in (34) for Δ_0. Figure 6 also shows that for larger and larger

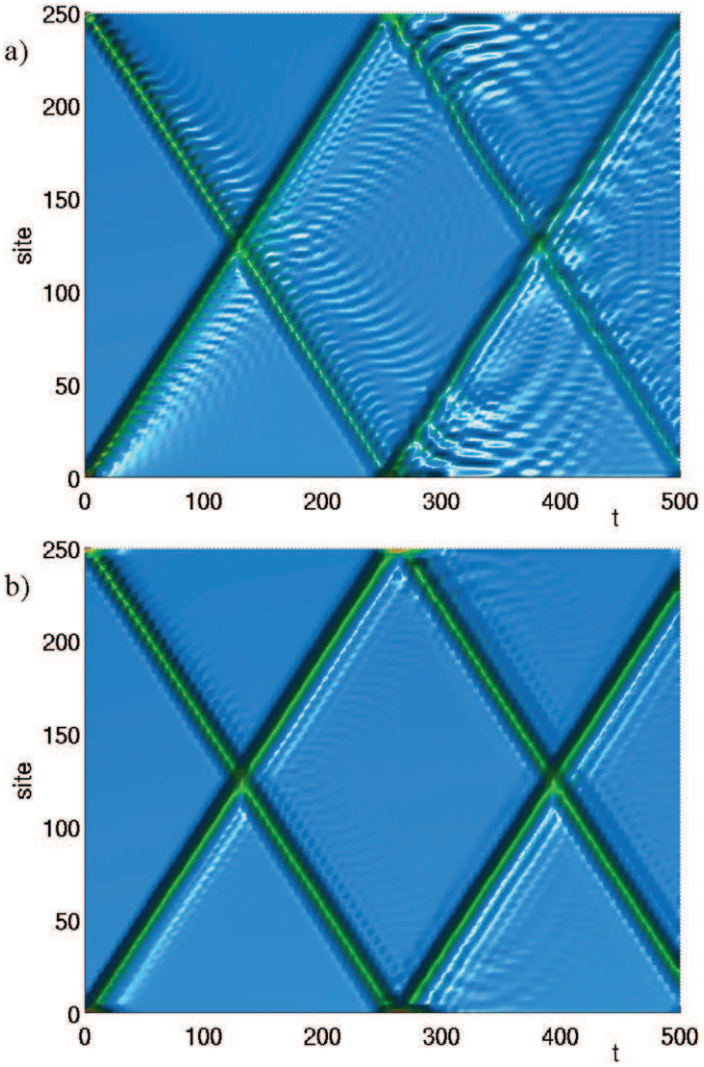

Figure 5. Dynamics of the magnetization $\sigma_i^z(t)$ at time t and site i when (a) $j_0 = 1$ and (b) $j_0 = j_0^{\text{opt}}$. The initial state of the whole system is $|\uparrow\rangle\otimes|\downarrow\downarrow\cdots\downarrow\rangle\otimes|\uparrow\rangle$ and the length of the chain is $N+2=250$.

N the maximal amplitude u_{opt} does not decrease towards zero, but rather tends to a constant value of about 0.85, which is surprisingly high, as, e.g., it corresponds to an average fidelity $\overline{\mathcal{F}}_{\text{AB}}(t^*) \gtrsim 0.9$. This can indeed be proven: we show in appendix B that in the limit of $N \to \infty$ the optimized amplitude tends to $u_{\text{opt}} = 0.8469$. Basically, this tells us that it is possible to transmit quantum states with very good quality also over macroscopic distances. From (B.14) we can derive the asymptotic behaviour of the optimal coupling

$$j_0^{\text{opt}} \simeq 1.030\, N^{-1/6}. \tag{35}$$

In the optimal ballistic case, the channel initialization is not crucial, as different initial states satisfying (22) give rise to almost the same dynamics as discussed at the end of section 3.2. In fact, the term $C_{N+1}(t)$ entering (15) essentially embodies the effect of channel initialization and it is expected to be small at t^*. This is apparent in figure 7, where for $j_0 = j_0^{\text{opt}}$, $C_{N+1}(t^*)$ stays well below 0.1 for N as long as 1000.

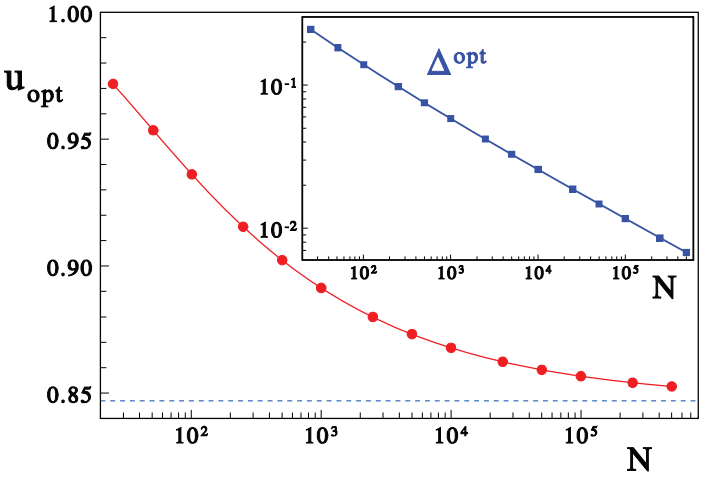

Figure 6. Behaviour of the maximum attainable amplitude $u_{\rm opt}$ and (inset) of the corresponding optimal value of $\Delta^{\rm opt}$ versus logarithm of the chain length N. The horizontal dashed line is the infinite N limit of $u_{\rm opt}$.

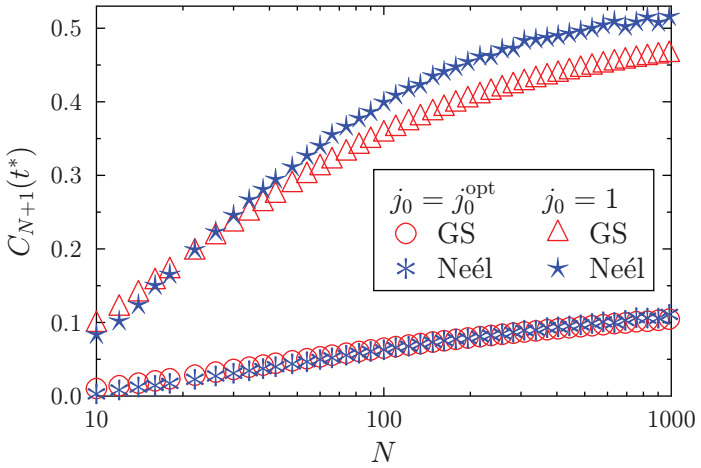

Figure 7. $C_{N+1}(t^*)$ for different initial states of the chain (ground state, antiferromagnetic Neél state and series of singlets [31]) when $j_0 = j_0^{\rm opt}$ and $j_0 = 1$. The results for a series of singlets are numerically indistinguishable from those with the Neél state.

The transmitted entanglement, as measured by the concurrence (20), is shown in figure 8 as a function of j_0 and t, with the channel initially prepared in its ground state. As expected, the peak of the transmitted concurrence is observed for $j_0 = j_0^{\rm opt}$; away from $j_0^{\rm opt}$ the quality of transmission falls down because $u(t^*)$ decreases and, accordingly, $v(t^*)$ is allowed to increase. In fact, in the nonoptimal ballistic case the quality of entanglement transfer does depend on the initial state of the channel [31, 33]; for instance, when $j_0 = 1$ and the chain is initially in its ground state, the contribution of the overlap terms $\mathrm{Tr}[\rho^{\Gamma} c_j^{\dagger} c_{j'}]$ in (16) is not quenched by the dynamical prefactors, and higher values of $C_{N+1}(t^*)$ (see figure 7) inhibit the transmission of entanglement even if $u(t^*) \neq 0$.

The effect of the optimization of j_0 is clearly evident in the time behaviour, reported in figure 9, of the minimum fidelity $\mathcal{F}_{\rm AB}^{\rm min}(t)$: its peak for $j_0^{\rm opt}$ occurs at the arrival time

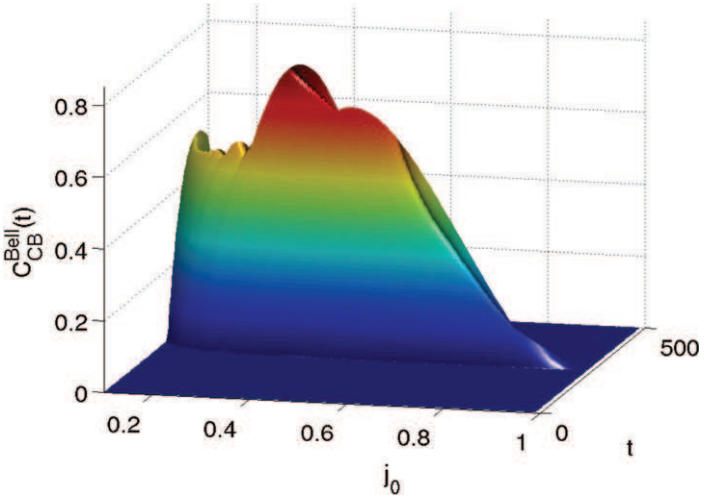

Figure 8. Evolution of the concurrence $\mathcal{C}^{\mathrm{Bell}}_{\mathrm{CB}}$ versus j_0 and t. The length of the chain is $N+2=250$.

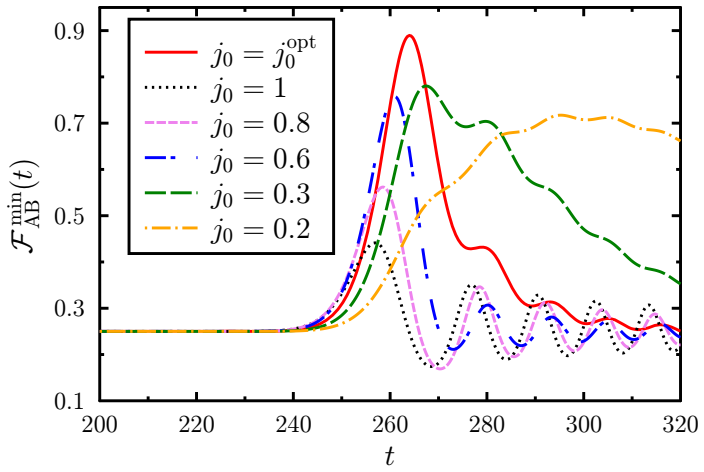

Figure 9. Minimum fidelity versus time for different values of j_0. The length of the chain is $N+2=251$ and $j_0^{\mathrm{opt}}=0.422$.

$t^*=N+3+s$ with a time delay s that agrees with the asymptotic value $s\simeq 2.29\,N^{1/3}$ derived in appendix B. The 'reading time', i.e. the time interval during which the qubit B remains in the transferred quantum state, is $t_{\mathrm{R}}\simeq\Delta^{-1}$, as the same figure also shows; note that, in the optimal case, t_{R} increases with N according to the asymptotic behaviour $t_{\mathrm{R}}\simeq 1.89\,N^{1/3}$.

6. Conclusions

In this paper, we have shown that high-quality quantum state and entanglement transfer between two qubits A and B is obtained through a uniform XX channel of arbitrary length N by a proper choice of the interaction j_0 between the channel and the qubits. The value of such interaction is found to control the transfer regime of the channel, which varies, as j_0 increases, from the Rabi-like one, characterized by a very long transmission time, to an intermediate regime, which turns useless for the purpose of quantum communication and finally becomes ballistic for j_0 of the order of the intrachannel interaction.

In order to get coherent transfer in the ballistic regime, it is desirable that the k-density of the travelling wavepacket generated by Alice's initialized qubit A be narrow and concentrated in the linear zone of the dispersion relation, i.e. with equispaced frequencies. As the parameter j_0 controls both the width of the k-density and the spacings of the frequencies entering the dynamics, one can improve the transmission quality up to a best balance obtained for an optimal value $j_{\rm opt}(N)$, which for large N behaves as $j_{\rm opt}(N) \simeq 1.03\, N^{-1/6}$. Remarkably, we found that for such a choice the quantum-state-transfer quality indicators are very high and, indeed, have a lower bound for $N \to \infty$ that still lets quantum-information tasks be efficiently performed: e.g. the average fidelity of state transmission is larger than 90%. Moreover, as remarked in section 4.2, a fine-tuning of j_0 (and/or N) is not required, since even a relatively large mismatch from the optimal value does not affect significantly the quality of transmission.

The ballistic regime ensures fast transmission on a time scale of the order of N, at variance with the Rabi-like regime, and in the optimal case the reading time increases as $N^{1/3}$. It is also to be noted that, if experimental settings constrain to a given value $j_0^{\rm exp}$, one can still optimize the chain length in such a way that $j_0^{\rm exp} = j_0^{\rm opt}(N)$. The only requirement on the initial state of the receiving qubit B and of the spin bus is to possess $U(1)$ symmetry, a condition that can be fulfilled by several configurations concerning the spin bus, ranging from the fully polarized state to the highly entangled ground state. If a large magnetic field can be switched on during the initialization procedure (in order to fully polarize the channel) and switched off as soon as the transmission starts, then from our analytical treatment it emerges that temperature is not a major issue as far as the dynamical evolution of the channel is concerned, although low temperatures are obviously necessary to protect the qubits from phase and amplitude damping due to the solid-state environment. To judge if the proposed scheme identifies a reasonable experimental framework, let us estimate the magnitude of the involved physical quantities. Consider a solid-state implementation with lattice spacing of about 10 Å and intrachain exchange $J \simeq 10^2$ K. A quantum state will then be transferred with fidelity 90% along a channel of length 1 cm ($N \simeq 10^7$) using $j_0 \simeq 1.03\, N^{-1/6}\, J \simeq 7.0$ K, with transmission time $t = N\hbar/(k_{\rm B} J) \simeq 0.75\, \mu$s and reading time $t_{\rm R} \simeq 1.9\, N^{1/3}\, \hbar/(k_{\rm B} J) \simeq 0.03$ ns.

Acknowledgments

We acknowledge financial support from the Italian Ministry of University in the framework of the 2008 PRIN programme (contract no. 2008PARRTS 003). LB and PV thank Dr A Bayat and Professor S Bose for useful discussions, and TJGA thanks ISC-CNR for the kind hospitality.

Appendix A. Quasi-uniform tridiagonal matrices

The matrix Ω appearing in (10) can be written as $\Omega = -h - \frac{1}{2}\mathcal{M}$, where

$$\mathcal{M}(x, y) = \begin{pmatrix} x & y & & & & & \\ y & 0 & 1 & & & & \\ & 1 & 0 & 1 & & & \\ & & \ddots & \ddots & \ddots & & \\ & & & 1 & 0 & 1 & \\ & & & & 1 & 0 & y \\ & & & & & y & x \end{pmatrix} \tag{A.1}$$

is a square tridiagonal matrix of dimension $M = N + 2$, and $x = 2(h_0 - h)$ and $y = j_0$. This real symmetric matrix is diagonalized by an orthogonal matrix $O(x, y)$,

$$\sum_{i,j=1}^{M} \mathcal{O}_{ki} \mathcal{M}_{ij} \mathcal{O}_{k'j} = \lambda_k \, \delta_{kk'}, \tag{A.2}$$

and it is known that (i) if $y \neq 0$ the eigenvalues are nondegenerate [34] and (ii) the eigenvectors corresponding to the eigenvalues ordered in descending order are alternately symmetric and skew symmetric [35], i.e.

$$\mathcal{O}_{ki} = \pm \, \mathcal{O}_{k,M+1-i}. \tag{A.3}$$

The eigenvalues are the roots of the associated characteristic polynomial

$$\chi_M(\lambda; x, y) \equiv \det[\lambda - \mathcal{M}(x, y)]. \tag{A.4}$$

In the fully uniform case the characteristic polynomial is $\eta_M(\lambda) \equiv \chi_M(\lambda; 0, 1)$ and one easily obtains the recursion relation

$$\eta_M = \lambda \, \eta_{M-1} - \eta_{M-2}, \tag{A.5}$$

which can be solved in terms of Chebyshev polynomials of the second kind,

$$\eta_M = \frac{\sin(M+1)k}{\sin k}, \tag{A.6}$$

where

$$\lambda \equiv 2 \, \cos k, \tag{A.7}$$

so the eigenvalues of $\mathcal{M}(0, 1)$ correspond to M discrete values of k,

$$k = \frac{\pi \, n}{M+1} \quad (n = 1, \ldots, M); \tag{A.8}$$

the corresponding eigenvectors are

$$\mathcal{O}_{ki}(0, 1) = \sqrt{\tfrac{2}{M+1}} \, \sin ki. \tag{A.9}$$

The general determinant (A.4) can be expressed in terms of η_M's by expanding it in the first and then in the last column,

$$\chi_M = (\lambda^2 - 2x\lambda + x^2) \, \eta_{M-2} - 2y^2(\lambda - x) \, \eta_{M-3} + y^4 \, \eta_{M-4}, \tag{A.10}$$

and using (A.5) one can eliminate the explicit appearances of λ,

$$\chi_M = \eta_M - 2x \, \eta_{M-1} + x^2 \, \eta_{M-2} + (1 - y^2)[2 \, \eta_{M-2} - 2x \, \eta_{M-3} + (1 - y^2) \, \eta_{M-4}]. \tag{A.11}$$

By rewriting (A.6) as $\sin k \; \eta_M = \mathrm{Im}[\mathrm{e}^{\mathrm{i}(M+1)k}]$ and defining

$$z^2 \equiv 1 - y^2, \quad z_k^2 \equiv z^2 \, \mathrm{e}^{-2\mathrm{i}k}, \quad x_k \equiv x \, \mathrm{e}^{-\mathrm{i}k}, \tag{A.12}$$

$$u_k \equiv 1 - x_k + z_k^2 = \mathrm{e}^{-\mathrm{i}k}\{[(2 - y^2) \cos k - x] + \mathrm{i} \, y^2 \sin k\}, \tag{A.13}$$

equation (A.11) takes the form

$$\sin k \; \chi_M(k) = \mathrm{Im}\{\mathrm{e}^{\mathrm{i}(M+1)k} \; u_k^2\}. \tag{A.14}$$

The secular equation $\mathrm{Im}\{\mathrm{e}^{\mathrm{i}(M+1)k}u_k^2\}=0$ entails that when k corresponds to an eigenvalue the quantity in braces is real and equal to either $\pm|u_k|^2$; setting $u_k \equiv |u_k|\,\mathrm{e}^{-\mathrm{i}\varphi_k}$ it turns into $\sin[(M+1)k-2\varphi_k]=0$, with the phase shifts

$$\varphi_k = k - \tan^{-1}\frac{y^2\sin k}{(2-y^2)\cos k - x}, \tag{A.15}$$

so the M eigenvalues correspond to

$$k_n = \frac{\pi\, n + 2\varphi_{k_n}}{M+1}, \quad (n=1,\ldots,M). \tag{A.16}$$

We are interested in the squared components of the first column of the diagonalizing matrix $\mathcal{O}_{ki}$, which can be expressed as [34]

$$\mathcal{O}_{k1}^2 = \frac{\xi_{M-1}(\lambda_k)}{\partial_\lambda \chi_M(\lambda_k)} = -\frac{2\sin k\;\xi_{M-1}(k)}{\partial_k \chi_M(k)}, \tag{A.17}$$

where k assumes the values (A.16) and $\xi_{M-1}(\lambda; x, y)$ is the characteristic polynomial associated with the first minor matrix $\mathcal{M}^{(11)}$ that, expanded in the last column and using (A.5), reads

$$\begin{aligned}\xi_{M-1} &\equiv \det[\lambda - \mathcal{M}^{(11)}(x,y)] = (\lambda - x)\,\eta_{M-2} - y^2\,\eta_{M-3}\\ &= \eta_{M-1} - x\,\eta_{M-2} + (1-y^2)\,\eta_{M-3}.\end{aligned} \tag{A.18}$$

Then the numerator of (A.17) is

$$\sin k\;\xi_{M-1} = \mathrm{Im}\{\mathrm{e}^{\mathrm{i}Mk}u_k\}, \tag{A.19}$$

while from (A.14) one has

$$\begin{aligned}\sin k\;\partial_k\chi_M(k) &= (M+1)\,\mathrm{Re}\{\mathrm{e}^{\mathrm{i}(M+1)k}u_k^2\} + 2\,\mathrm{Im}\{\mathrm{e}^{\mathrm{i}(M+1)k}\,u_k u_k'\}\\ &= \mathrm{e}^{\mathrm{i}(M+1)k}u_k^2(M+1+2\,\mathrm{Im}\{u_k'/u_k\})\\ &= \mathrm{e}^{\mathrm{i}(M+1)k}u_k^2(M+1-2\varphi_k');\end{aligned} \tag{A.20}$$

indeed, the argument of Re is real and $u_k'/u_k = \partial_k \ln u_k = \partial_k|u_k| - \mathrm{i}\varphi_k'$. Hence, (A.17) becomes

$$\mathcal{O}_{k1}^2 = \frac{2}{M+1-2\varphi_k'}\;\frac{y^2\sin^2 k}{[(2-y^2)\cos k - x]^2 + y^4\sin^2 k}. \tag{A.21}$$

Note that for $x=0$ this expression is in agreement with [3] and that the term with φ_k' becomes irrelevant for large M. In the most common case $x < 2-y^2$, the maximum k_0 of $\mathcal{O}_{k1}^2$ is located at

$$k_0 = \cos^{-1}\frac{x}{2-y^2}, \tag{A.22}$$

and the corresponding 'eigenvalue' is

$$\lambda_0 = 2\cos k_0 = \frac{2x}{2-y^2} \tag{A.23}$$

so that the 'energy' of the k_0 mode increases linearly with x. Expanding $\mathcal{O}_{k1}^2$ around k_0, the leading behaviour is found to be a Lorentzian,

$$\mathcal{O}_{k1}^2 \simeq \frac{2}{M+1}\;\frac{y^2}{y^4 + [(2-y^2)^2 - x^2](k-k_0)^2}, \tag{A.24}$$

whose half-width at half maximum (HWHM) is given by

$$\Delta \simeq \frac{y^2}{\sqrt{(2-y^2)^2 - x^2}}. \tag{A.25}$$

When x and y are small, $k_0 \simeq (\pi - x)/2$ and $\Delta \simeq y^2/2$, so x rules the position of the peak, while y determines its width.

Appendix B. Large-N limit of the amplitude

The transition amplitude (28) in the case of odd $N = 2M - 1$ reads

$$u(t) = \sum_{m=-M}^{M} \frac{\Delta(1+\Delta)}{N+3+2\varphi'_{q_m}} \frac{\mathrm{e}^{\mathrm{i}(\pi m - t \sin q_m)}}{\Delta^2 + \tan^2 q_m}, \tag{B.1}$$

where the summation has been made symmetric through the change of variable $q = \pi/2 - k$. The shift equation (25) turns into

$$\pi\, m = (N+3)\, q_m + 2\varphi_{q_m}, \tag{B.2}$$

with

$$\varphi_q = \tan^{-1} \frac{\tan q}{\Delta} - q. \tag{B.3}$$

In the limit $N \to \infty$ one can write the sum as an integral setting

$$\sum_m \frac{1}{N+3+2\varphi'_{q_m}} (\cdots) \longrightarrow \int \frac{\mathrm{d}q}{\pi} (\cdots). \tag{B.4}$$

As we are interested in the region of the optimal value of $\Delta \sim N^{-1/3} \to 0$, we have

$$u_\infty(t) = \lim_{N\to\infty} \Delta \int_{-\frac{\pi}{2}}^{\frac{\pi}{2}} \frac{\mathrm{d}q}{\pi} \frac{\mathrm{e}^{\mathrm{i}[(N+3)q + 2\varphi_q - t \sin q]}}{\Delta^2 + \tan^2 q}. \tag{B.5}$$

Writing the arrival time as $t = N + 3 + s$, where s is the arrival delay, one has then

$$u_\infty(t) = \lim_{t\to\infty} \Delta \int_{-\frac{\pi}{2}}^{\frac{\pi}{2}} \frac{\mathrm{d}q}{\pi} \frac{\mathrm{e}^{\mathrm{i}[t(q - \sin q) - sq + 2\varphi_q]}}{\Delta^2 + \tan^2 q}. \tag{B.6}$$

The relevant q's are of the order of $\Delta \sim N^{-1/3} \to 0$, so we change to $q = \Delta x$, with x of the order of 1; keeping the leading terms for $\Delta \to 0$,

$$t\,(q - \sin q) \longrightarrow \frac{t\Delta^3}{6} x^3, \tag{B.7}$$

$$\varphi_q \longrightarrow \tan^{-1} x, \tag{B.8}$$

$$\frac{\Delta\, \mathrm{d}q}{\Delta^2 + \tan^2 q} \longrightarrow \frac{\mathrm{d}x}{1+x^2}, \tag{B.9}$$

and defining the rescaled counterparts of the arrival time $t \simeq N$ and of the delay $s \sim N^{1/3}$,

$$\tau \equiv \frac{\Delta^3}{6} t, \quad \sigma \equiv \Delta s; \tag{B.10}$$

the final asymptotic expression is

$$u_\infty(\tau,\sigma) = \int_{-\infty}^{\infty} \frac{\mathrm{d}x}{\pi} \frac{\mathrm{e}^{\mathrm{i}(\tau x^3 - \sigma x + 2\tan^{-1} x)}}{1+x^2}, \tag{B.11}$$

which can also be rewritten in the form of a simple summation of phases by introducing the variable $z = \tan^{-1} x$,

$$u_\infty(\tau,\sigma) = \frac{2}{\pi} \int_0^{\frac{\pi}{2}} \mathrm{d}z \ \cos(\tau \tan^3 z - \sigma \tan z + 2z). \tag{B.12}$$

As in the finite-N case, one has to maximize $u_\infty(\tau,\sigma)$ by finding the optimal values of σ and τ. For $\tau = 0$ it is easy to evaluate (B.11) analytically,

$$u_\infty(0,\sigma) = 2\,\mathrm{e}^{-\sigma}\sigma; \tag{B.13}$$

it is maximal for $\sigma = 1$, giving $u(0,1) = 2\,\mathrm{e}^{-1} \simeq 0.736$, to be regarded as a lower bound to the overall maximum of $u_\infty(\tau,\sigma)$. The overall maximization has been performed numerically using (B.12). It turns out that the maximum corresponds to $\sigma = 1.2152$ and $\tau = 0.024\,83$, and amounts to $u_\infty(0.024\,83, 1.215\,2) = 0.846\,90$, in agreement with the behaviour shown in figure 6. The resulting scaling, from (B.10), tells that asymptotically

$$\Delta \simeq 0.530\ N^{-1/3}, \quad s \simeq 2.29\ N^{1/3}. \tag{B.14}$$

References

[1] Bose S 2007 Quantum communication through spin chain dynamics: an introductory overview *Contemp. Phys.* **48** 13

[2] Bose S 2003 Quantum communication through an unmodulated spin chain *Phys. Rev. Lett.* **91** 207901

[3] Wójcik A, Łuczak T, Kurzyński P, Grudka A, Gdala T and Bednarska M 2005 Unmodulated spin chains as universal quantum wires *Phys. Rev.* A **72** 034303

[4] Apollaro T J G and Plastina F 2006 Entanglement localization by a single defect in a spin chain *Phys. Rev.* A **74** 062316

[5] Campos Venuti L, Giampaolo S M, Illuminati F and Zanardi P 2007 Long-distance entanglement and quantum teleportation in XX spin chains *Phys. Rev.* A **76** 052328

[6] Giampaolo S M and Illuminati F 2010 Long-distance entanglement in many-body atomic and optical systems *New J. Phys.* **12** 025019

[7] Banchi L, Apollaro T J G, Cuccoli A, Vaia R and Verrucchi P 2010 Optimal dynamics for quantum-state and entanglement transfer through homogeneous quantum systems *Phys. Rev.* A **82** 052321

[8] Ramanathan C, Cappellaro P, Viola L and Cory D G 2011 Dynamics of magnetization transport in a one-dimensional spin system *New J. Phys.* **13** 103015

[9] Zwick A and Osenda O 2011 Quantum state transfer in a XX chain with impurities *J. Phys. A: Math. Theor.* **44** 105302

[10] Christandl M, Datta N, Dorlas T C, Ekert A, Kay A and Landahl A J 2005 Perfect transfer of arbitrary states in quantum spin networks *Phys. Rev.* A **71** 032312

[11] Karbach P and Stolze J 2005 Spin chains as perfect quantum state mirrors *Phys. Rev.* A **72** 030301

[12] Di Franco C, Paternostro M and Kim M S 2008 Perfect state transfer on a spin chain without state initialization *Phys. Rev. Lett.* **101** 230502

[13] Zwick A, Álvarez G A, Stolze J and Osenda O 2011 Robustness of spin-coupling distributions for perfect quantum state transfer *Phys. Rev.* A **84** 022311

[14] Hu M L and Lian H L 2009 State transfer in intrinsic decoherence spin channels *Eur. Phys. J.* D **55** 711

[15] Fel'dman E B, Kuznetsova E I and Zenchuk A I 2010 High-probability state transfer in spin-1/2 chains: analytical and numerical approaches *Phys. Rev.* A **82** 022332
[16] Kay A 2009 Interfacing with Hamiltonian dynamics *Phys. Rev.* A **79** 042330
[17] Pemberton-Ross P J, Kay A and Schirmer S G 2010 Quantum control theory for state transformations: dark states and their enlightenment *Phys. Rev.* A **82** 042322
[18] Osborne T J and Linden N 2004 Propagation of quantum information through a spin system *Phys. Rev.* A **69** 052315
[19] Yadsan-Appleby H and Osborne T J 2011 Achievable qubit rates for quantum information wires arXiv:1102.2427
[20] Yung M H and Bose S 2005 Perfect state transfer, effective gates and entanglement generation in engineered bosonic and fermionic networks *Phys. Rev.* A **71** 032310
[21] Gualdi G, Kostak V, Marzoli I and Tombesi P 2008 Perfect state transfer in long-range interacting spin chains *Phys. Rev.* A **78** 022325
[22] Yao N Y, Jiang L, Gorshkov A V, Gong Z-X, Zhai A, Duan L-M and Lukin M D 2011 Robust quantum state transfer in random unpolarized spin chains *Phys. Rev. Lett.* **106** 040505
[23] Banchi L, Bayat A, Verrucchi P and Bose S 2011 Nonperturbative entangling gates between distant qubits using uniform cold atom chains *Phys. Rev. Lett.* **106** 140501
[24] Nielsen M A and Chuang I L 2000 *Quantum Information and Computation* (Cambridge: Cambridge University Press)
[25] Di Franco C, Paternostro M, Palma G M and Kim M S 2007 Information-flux approach to multiple-spin dynamics *Phys. Rev.* A **76** 042316
[26] Wootters W K 1998 Entanglement of formation of an arbitrary state of two qubits *Phys. Rev. Lett.* **80** 2245
[27] Nielsen M A 2002 A simple formula for the average gate fidelity of a quantum dynamical operation *Phys. Lett.* A **303** 249
[28] Horodecki M, Horodecki P and Horodecki R 1999 General teleportation channel, singlet fraction and quasidistillation *Phys. Rev.* A **60** 1888
[29] Lieb E, Schultz T and Mattis D 1961 Two soluble models of an antiferromagnetic chain *Ann. Phys.* **16** 407
[30] Cozzini M, Giorda P and Zanardi P 2007 Quantum phase transitions and quantum fidelity in free fermion graphs *Phys. Rev.* B **75** 014439
[31] Bayat A, Banchi L, Bose S and Verrucchi P 2011 Initializing an unmodulated spin chain to operate as a high quality quantum data-bus *Phys. Rev.* A **83** 062328
[32] Markiewicz M and Wieśniak M 2009 Perfect state transfer without state initialization and remote collaboration *Phys. Rev.* A **79** 054304
[33] Bayat A and Bose S 2010 Information-transferring ability of the different phases of a finite XXZ spin chain *Phys. Rev.* A **81** 012304
[34] Parlett B N 1998 *The Symmetric Eigenvalue Problem* (Philadelphia, PA: SIAM)
[35] Cantoni A and Butler P 1976 Eigenvalues and eigenvectors of symmetric centrosymmetric matrices *Linear Algebra Appl.* **13** 275